CHARACTERIZATION AND CORROSION BEHAVIOUR OF 96.5Sn-3.0Ag-0.5Cu SOLDER ON Cu SUBSTRATE AT DIFFERENT REFLOW REACTIONS

by

LEE LIU MEI

Thesis submitted in fulfillment of the requirements for the degree of Master of Science

January 2013

ACKNOWLEDGEMENT

I would like to express my deepest and sincere gratitude to my supervisor, Assoc. Prof. Dr. Ahmad Azmin Mohamad for his valuable contributions to this work, continuous support, enthusiasm, and patience. His guidance is well-appreciated and I deeply believe that one could not possibly reach this far without such respectable supervision. Throughout the project, I have learnt a lot of priceless lessons from him.

Besides, my utmost thankfulness is expressed to the Universiti Sains Malaysia for the financial support via the Fellowship programme, the Short Term Grant (60311005) and RU Grant (814112). Likewise, I would also like to extend my gratitude to the School of Materials and Mineral Resources Engineering, Universiti Sains Malaysia for accommodating me during the conduct of my studies and for allowing me to use their facilities and equipment. Special thanks to all academic and technical staffs for their contributions and tremendous assistance.

Also, I would like to express my deep appreciation to Muhammad Firdaus Mohd Nazeri, Siti Salwa Alias, Muhammad Ghaddafy Affendy and Mohamad Najmi Masri, who have been giving me pieces of advice and encouragement unconditionally. Finally, I would like to thank my beloved family and friends for the prayers, support, encouragements and inspiration amidst the challenges.

LEE LIU MEI

January 2013

TABLES OF CONTENTS

Acknowledgement	ii
Tables of Contents	iii
List of Figures	v
List of Tables	xv
List of Abbreviations	xvi
Abstrak	xviii
Abstract	xx

CHAPTER 1 INTRODUCTION

1.0 Introduction	1
1.1 Problem Statement	2
1.2 Objectives	6
1.3 Scope of Work	6

CHAPTER 2 LITERATURE REVIEW

2.0 Introduction	8
2.1 Soldering in Electronics Technology	8
2.2 Thin Film Solders	13
2.3 Sn-Ag-Cu Solders	16
2.3.1 Phase Diagram of Sn-Ag-Cu Solders	17
2.4 Intermetallic Compound of Sn-Ag-Cu Solders with Cu Substrate	20
2.4.1 Structural Phases of Sn-Ag-Cu/Cu	23

2.4.2 Morphology Evolution of Interfacial Intermetallic Compounds 25

2.4.3 Formation and Growth Kinetics of Interfacial Intermetallic Compounds 30

2.4.4 Effects of Reflow Temperature and Time on Interfacial Intermetallic Compounds 34

2.5 Corrosion as Reliability Consideration 41

2.5.1 Corrosion in Electronics 41

2.6 Potentiodynamic Polarization Scan 45

2.7 Electrochemical Properties of Sn-Ag-Cu Solders 49

CHAPTER 3 EXPERIMENTAL

3.0 Introduction 61

3.1 Material and Experiment Apparatus 61

3.2 Preparation of Sn-Ag-Cu Thin Film 62

3.3 Solder Reflow and Intermetallic Compound Formation 63

3.4 Potentiodynamic Polarization Test in Potassium Hydroxide 65

3.4.1 Electrolyte Preparation 65

3.4.2 Working Sample Preparation 65

3.4.3 Potentiodynamic Polarization Test 66

3.5 Materials Characteristics 68

3.5.1 Phase Determination 68

3.5.2 Microstructural and Compositional Analysis 68

3.5.3 Analytical Characteristics 69

3.6 Flow Chart of the Experimental 69

CHAPTER 4 RESULTS AND DISCUSSION

4.0 Introduction 70

4.1 Characterization of Sn-3.0Ag-0.5Cu Thin Film on Cu Substrate and Intermetallic Compounds after Solder Reflow 70

4.1.1 Surface Appearance 70

4.1.2 Phase Determination 73

4.1.3 Morphology Evolution 79

4.1.4 Intermetallic Compound Layer Thickness as Function of Reflow Temperature and Time 87

4.2 Electrochemical Analysis 89

4.2.1 Potentiodynamic Polarization Curves 90

4.2.2 Structural Properties 96

4.2.3 Microstructural Properties 98

4.2.4 Corrosion Mechanism of Thin Film 103

CHAPTER 5 CONCLUSION AND RECOMMENDATIONS

5.0 Conclusion 106

5.1 Recommendation 108

References 110

Appendices

List of publication

LIST OF FIGURES

		Page
Figure 2.1	Solder wetting process: (a) solid solder on the base metal, (b) liquid solder spreading over base metal during soldering, (c) base metal dissolving in liquid solder, and (d) base metal reacting with liquid solder to form intermetallic compound layer (modified from Lea, 1988).	9
Figure 2.2	Cross-section of (a) a pin through hole connection of a microelectronics component on a printed wiring board, (b) a surface mount connection of a microelectronics component with leads on a printed wiring board, and (c) a ball grid array (BGA)microelectronics component (Abtew and Selvaduray, 2000).	11
Figure 2.3	Cross-section of a flip chip connection (Abtew and Selvaduray, 2000).	12
Figure 2.4	Illustration of fluxless bonding with a thin Cu_3Sn layer as the oxidation barrier (Liu et al., 2010a).	15
Figure 2.5	The scheme of diffusion soldering for Cu/Ti/Si and Au/Cu/Al_2O_3 with Sn interlayers (Liang et al., 2003).	16
Figure 2.6	(a) Ternary phase diagram of Sn-Ag-Cu solder alloy and (b) liquidus surfaces of Sn-Ag-Cu phase diagrams at the Sn-rich corner (Moon et al., 2000).	18
Figure 2.7	Binary Ag-Sn system (Massalski and Okamoto, 1990).	19
Figure 2.8	Cu-Sn binary phase diagram (Massalski and Okamoto, 1990).	20

Figure 2.9 Scheme of the interfacial reaction of SAC305/Cu during solder reflow; (a) dissolution of Cu substrate, (b) supersaturation of molten solder layer with Cu, (c) formation of scallop type Cu_6Sn_5 at interface, and (d) Cu_3Sn emerges between Cu_6Sn_5/Cu with prolonged soldering (modified from Kivilahti, 2002). 23

Figure 2.10 XRD patterns of interfacial IMC at SAC305/Cu joints reflowed at 250 ºC for 30 s (Liu et al., 2010b). 24

Figure 2.11 XRD spectrums of the IMCs for SAC305/Cu (Wang et al., 2007). 25

Figure 2.12 SEM-BS image of the solder alloy–Cu joint showing different regions Sn–Ag–Cu alloy, with region (C): Sn (~96.5) with Ag, (D): Sn (~53.9) and Ag (~46.1) and (E): Ag (~34.5), Sn (~61.0) and Cu (~4.5) (Kar et al., 2007). 26

Figure 2.13 Typical SEM image of SAC305 solder joints with Cu (modified from Kim et al., 2003). 27

Figure 2.14 SEM micrographs of the Cu/Sn–Ag–Cu/Cu joint reflowed at 250 ◦C for 60 s: (a) entire solder joint, (b) top interface, (c) solder matrix, and (d) bottom interface (Yoon and Jung, 2008). 28

Figure 2.15 Back-scattered electron image of Sn-0.5Cu alloy: (a) 1.0 wt% Ag, (b) 2.0 wt% Ag, (c) 3.0 wt% Ag, and (d) 4.0 wt% Ag (Reid et al., 2008). 29

Figure 2.16 Morphologies of Ag_3Sn compound under varying Ag concentration with (a) 1.0-3.0Ag alloying and (b) 4.0Ag alloying (modified from (Reid et al., 2008). 29

Figure 2.17 Schematic diagram of the growth mechanism of Cu_6Sn_5 at the Sn-Ag-Cu/Cu interface: (a) individual Cu_6Sn_5 grains at interface, (b) Cu_6Sn_5 growth along the interface, (c) ripening process resulted in scallop Cu_6Sn_5, and (d) coarsening of scallop Cu_6Sn_5 (modified from Görlich et al., 2005; Choi and Lee, 2000). 31

Figure 2.18 Schematic diagram of IMCs thickness measurements with T_1 as the thickness of Cu_6Sn_5 and T_2 represents the thickness of Cu_3Sn. 34

Figure 2.19 Intermetallic compound found at various soldering conditions (Mookam and Kanlayasiri, 2011). 36

Figure 2.20 (a) The thickness of IMC layer under varying soldering time and (b) the growth mechanisms of IMC layer during soldering process (Yu and Wang, 2008). 37

Figure 2.21 Cross-sectional microstructure of (a) Sn–3.5Ag, (b) Sn–3.5Ag–0.7Cu, (c) Sn–3.5Ag–1.7Cu, and (d) Sn–4.0Cu–0.5Ag after soldering for 30 s (Yu and Wang, 2008). 38

Figure 2.22 The microstructure of the solder joints after soldering for 600 s: (a) Sn–3.5Ag, (b) Sn–3.5Ag–0.7Cu, (c) Sn–3.5Ag–1.7Cu, and (d) Sn–0.5Ag–4.0Cu (Yu and Wang, 2008). 38

Figure 2.23	Growth mechanism of Cu-Sn IMCs at various reflow times: (a) formation of scalloped Cu_6Sn_5 at SAC305/Cu interfacial region, (b) appearance of Cu_3Sn between Cu_6Sn_5/Cu interface, and (c) increase of both Cu-Sn IMCs thickness with increased reflow times (modified from Yu and Wang, 2008).	39
Figure 2.24	High magnification SEM micrographs of the interfacial Cu-Sn intermetallic layer in Sn-3.5Ag solder joints reflowed at 250 ºC for: (a) 15, (b) 30, (c) 60, (d) 120, (e) 240, and (f) 360 s (Li and Chen, 2003).	40
Figure 2.25	Tarnishing. (a) tarnished lead (single pin); (b) tarnished spot on a gold lid surface (Tan, 1993).	43
Figure 2.26	Schematic structure of solder joints in a flip chip package (Li et al., 2008).	44
Figure 2.27	Schematic polarization curve of passivable metals. AB-Cathodic polarization; BJ-anodic polarization; BF-dissolution of working sample, FG- passivation in process, GH-establishment of passivation, and HJ- passivation breakdown (Wu et al., 2006).	47
Figure 2.28	Potentiodynamic polarization curves of Sn-26.1Pb and Sn–Ag–M (M = In, Bi, Cu) solder alloys in aerated 0.1 M NaCl solution (Rosalbino et al., 2008).	51
Figure 2.29	SEM–BSE micrograph of the Sn-3.1Ag-0.8Cu solder alloy after polarization test in 0.1 M NaCl solution (Rosalbino et al., 2008).	52

Figure 2.30 SEM–BSE micrograph of the Sn-2.9Ag-6.7Cu solder alloy after polarization test in 0.1 M NaCl solution (Rosalbino et al., 2008). 53

Figure 2.31 Schematic presentation of corrosion mechanism for SAC solder alloys: (a) absorption of chloride ions, (b) breakdown of film, (c) dissolution of SAC solder, and (d) formation of corrosion pit. 54

Figure 2.32 Potentiodynamic polarization curves of SAC305 and Sn–3.0Ag–3.0Cu solder alloys in aerated 0.1M NaCl solution (Rosalbino et al., 2009). 55

Figure 2.33 SEM-BSE micrographs of the corrosion products layer formed at the surface of (a) SAC305 and (b) Sn–3.0Ag–3.0Cu solder alloys after potentiodynamic polarization tests in aerated 0.1M NaCl solution (Rosalbino et al., 2009). 56

Figure 2.34 Potentiodynamic polarisation curves of Sn–Ag–Cu solder in 3.5 wt.% NaCl solution (Li et al., 2008). 56

Figure 2.35 Microstructure of the corrosion products on Sn-3.8Ag-0.7Cu solder after potentiodynamic polarisation with the scanning rate for (a) is 30 mV/min and (b) is 300 mV/min (Li et al., 2008). 57

Figure 2.36 SEM images of tin(II) oxide crystals on the surfaces of lead-free solder joints after corrosion: (a) Sn-3.5Ag-0.75Cu and (b) SAC305 (Chang et al., 2009). 58

Figure 2.37	SEM images of (a) tin surface together with a thick epitaxial oxide film and (b) different morphologies of the oxide grown underneath (Gervasi et al., 2007).	59
Figure 3.1	Sketch of thermal evaporator for SAC305 solder wire deposition on Cu plate.	63
Figure 3.2	Flow chart of solder reflow.	64
Figure 3.3	Schematic diagram of KOH electrolyte preparation.	65
Figure 3.4	Configuration of potentiodynamic polarization measurement.	67
Figure 3.5	Flow chart of polarization in 6 M KOH.	68
Figure 3.6	Flow Chart of Methodology.	69
Figure 4.1	(a) bare Cu substrate, (b) as-deposited SAC305, and (c) as-reflowed SAC305/C at 230 ºC for 30 s.	71
Figure 4.2	Directional deposition of SAC305 thin film.	72
Figure 4.3	XRD patterns from the top surface of (a) bare Cu, (b) pure SAC305 solder wire, and (c) as-deposited SAC305/Cu. The inserts of (d) and (e) represent the superimpose of detailed diffraction ή-Cu_6Sn_5 peaks at angle ranging from 30º to 44º for (b) and (c), respectively.	75

Figure 4.4 Detail of the diffraction pattern of (a) SAC305 solder wire and (b) SAC305 thin film. 76

Figure 4.5 XRD patterns from the top surface of as-reflowed SAC305/Cu at reflow temperature of (a) 230, (b) 240, (c) 250, and (d) 260 ˚C for 30 s. 78

Figure 4.6 FESEM micrographs of the top surface of (a) bare Cu plate, (b) SAC305 solder wire, (c) as-deposited SAC305/Cu, and (d) as-reflowed SAC305/Cu at different reflow temperatures (red arrows show the grain boundaries). The compositions (wt %) are obtained by EDX analysis (refer to Appendix II). 81

Figure 4.7 FESEM micrographs of the cross-sectional surface of (a) bare Cu plate, (b) as-deposited SAC305/Cu and as-reflowed SAC305/Cu at (c) 230, (d) 240, (e) 250, and (f) 260°C reflow temperatures. The compositions (wt %) are obtained by EDX analysis (refer to Appendix III). 82

Figure 4.8 FESEM micrographs of the SAC305/Cu as-reflowed joints at constant reflow temperature of 230 ºC for (a) 5, (b) 10, (c) 15, and (d) 20 s with alcoholic ferric chloride etching. The compositions (wt %) are obtained by EDX analysis (refer to Appendix IV). 86

Figure 4.9 Cu-Sn IMCs thickness as a function of reflow temperature in a 30 s reflow time. 87

Figure 4.10 IMC layer thickness vs. reflow time at a 230 ºC reflow temperature. 89

Figure 4.11	Potentiodynamic polarization curves of the bare Cu plate, as-deposited SAC305/Cu, and as-reflowed SAC305/Cu at 230 ℃ for 30 s after polarized in a 6 M KOH solution	91
Figure 4.12	Potentiodynamic polarization curves of the as-reflowed SAC305/Cu at reflow temperatures of 230, 240, 250, and 260 ℃ for 30 s after polarized in a 6 M KOH solution.	95
Figure 4.13	XRD patterns from the top surface of (a) bare Cu, (b) as-deposited SAC305/Cu, and as-reflowed SAC305/Cu at (c) 230, (d) 240, (e) 250, and (f) 260 ℃ for 30 s after the potentiodynamic polarization in 6 M KOH.	97
Figure 4.14	FESEM micrographs of the corroded top surface of (a) bare Cu plate and (b) as deposited SAC305/Cu after the potentiodynamic polarization in 6 M KOH. The compositions (wt %) are obtained by EDX analysis (refer to Appendix V).	98
Figure 4.15	FESEM micrographs of the corroded top surface of the as-reflowed SAC305/Cu at reflow temperatures of (a) 230, (b) 240, (c) 250, and (d) 260 °C for 30 s after the potentiodynamic polarization in 6 M KOH. The compositions (wt %) are obtained by EDX analysis (refer to Appendix VI).	100
Figure 4.16	FESEM micrographs of the cross-sectional surface of (a) bare Cu plate, (b) as-deposited SAC305/Cu and as-reflowed SAC305/Cu at (c) 230, (d) 240, (e) 250, and (f) 260 °C for 30 s reflow temperatures after the potentiodynamic polarization. The compositions (wt %) are obtained by EDX analysis (refer to Appendix VII).	101

Figure 4.17 Effect of Cu_6Sn_5 thickness on both E_{corr} and I_{corr} during polarization of as-reflowed SAC305/Cu at various reflow temperatures in 6 M KOH solution. 102

Figure 4.18 Corrosion mechanism of (a-b) as-deposited SAC305/Cu, (c-d) as-reflowed SAC305/Cu at temperature range of 230 -240 º C, and (e-f) as-reflowed SAC305/Cu at temperature range of 250-260 ºC. 104

LIST OF TABLES

		Page
Table 2.1	Thickness of intermetallic phases at various soldering conditions (Mookam and Kanlayasiri, 2011).	35
Table 2.2	Standard emf of metals (Jones, 1992).	49
Table 2.3	Electrochemical and corrosion tests of lead-free solders.	60
Table 4.1	Standard free energy of formation of oxides (per gram atom O basis) (Abtew and Selvaduray, 2000; Zhang et al., 2009).	73
Table 4.2	Corrosion parameters of bare Cu plate, as-deposited SAC305/Cu, and as-reflowed SAC305/Cu.	92
Table 4.3	Electrode potentials of solder elements (Fubin and Lee, 2006; Jones, 1992).	94

LIST OF ABBREVIATIONS

IMC	Intermetallic Compound
SAC305	Sn-3.0Ag-0.5Cu
KOH	Potassium hydroxide
PCB	Printed Circuit Board
PTH	Pin-Through-Hole
SMT	Surface Mount Technology
BGA	Ball Grid Array
SLID	Solid-Liquid Interdiffusion Bonding
IRL	Interfacial Reaction Layer
emf	electromotive force
QFP	Quad Flat Packs
FESEM	Field Emission Scanning Electron Microscopy
ICDD	International Center of Diffraction Data
Cl^-	Chloride ion
OH^-	Hydroxide ion
E_{corr}	Corrosion Potential
I_{corr}	Corrosion Current Density
I_c	Critical Current Density
I_p	Passivation Current Density
E_b	Breakdown Potential
SEM	Scanning Electron Microscopy

SEM-BSE	Scanning Electron Microscopy-Back Scattered Electron
TEM	Transmission Electron Microscopy
XRD	X-Ray Diffraction
IPC	International Printed Circuit

PENCIRIAN DAN KELAKUAN KAKISAN 96.5Sn-3.0Ag-0.5Cu PATERI ATAS SUBSTRAT CU PADA REAKSI ALIRAN PATERI YANG BERBEZA

ABSTRAK

Filem nipis 96.5Sn-3.0Ag-0.5Cu (SAC305) pateri mempamerkan ciri-ciri permukaan yang berbeza jika dibandingkan dengan pateri pukal konvensional. Dalam pateri filem nipis, permukaan sebenar terdiri daripada lapisan intermetalik sedangkan dalam kes pateri konvensional, lapisan intermetalik berlaku di rantau antara muka SAC305/Cu. Ini seterusnya menghasilkan mikrostruktur permukaan dan komposisi kimia yang berbeza. Selain itu, kajian teliti berkenaan SAC305 dalam ciri-ciri filem nipis adalah terhad. Oleh itu, Tindakbalas diantara filem nipis SAC305 pateri dan Cu substrat dikaji dengan aliran pateri pada pelbagai suhu dan masa. Pencirian struktur dan unsur menunjukkan kewujudan fasa Sn, Ag_3Sn, dan Cu_6Sn_5 pada filem nipis SAC305 yang didepositkan pada Cu substrat. Selepas aliran pateri, terdapat dua lapisan sebatian intermetalik. Lapisan atas ialah Cu_6Sn_5 dan mempunyai isipadu hampir secara eksklusif dalam keseluruhan, manakala Cu_3Sn muncul sebagai lapisan nipis yang seragam di bawahnya. Lapisan Cu_3Sn intermetalik bertambah dengan peningkatan suhu tetapi masih dalam ketebalan lapisan nipis SAC305. Kelakuan kakisan Cu, deposit SAC305/Cu and pateri SAC305/Cu dikaji melalui polarisasi potentiodynamic dalam 6 M larutan kalium hidroksida (KOH). Cu mempunyai ketahanan kakisan yang terbaik, manakala deposit SAC305/Cu mempunyai ketahanan kakisan yang terendah. Pateri SAC305/Cu yang mempunyai lapisan Cu_3Sn yang terdedah mempamerkan ketahanan kakisan yang baik berbanding dengan pateri SAC305/Cu yang mempunyai lapisan Cu_6Sn_5 terdedah. Semua sampel mengandungi produk kakisan oksida. Cu mematuhi struktur terkenal

dupleks Cu_2O/CuO, $Cu(OH)_2$. Bagi pateri SAC305/Cu, permukaan terkakis juga sebahagian besar terdiri daripada SnO and SnO_2.

CHARACTERIZATION AND CORROSION BEHAVIOUR OF 96.5Sn-3.0Ag-0.5Cu SOLDER ON Cu SUBSTRATE AT DIFFERENT REFLOW REACTIONS

ABSTRACT

96.5Sn-3.0Ag-0.5Cu (SAC305) thin film solder exhibits different surface characteristics if compared to conventional bulk solder. In thin film solder, the actual surface is comprised of intermetallic layers whereas in the case of conventional solder, the intermetallic layers happened at the interfacial region of solder/base metal. This in turn, resulted in different surface microstructure and chemical composition. Moreover, a subtle and unstudied aspect of SAC305 in thin film characteristics was limited. Thus, the effect of solder reflow conditions at various temperatures and times were investigated. Structural and elemental characterizations indicated that Sn, Ag_3Sn, and Cu_6Sn_5 were present in the as-deposited SAC305 thin film on Cu substrate. After solder reflow, SAC305 thin film was totally reacted and developed into Cu_6Sn_5 then Cu_3Sn. Cu_6Sn_5 is located almost exclusively in the volume, whereas Cu_3Sn appears as a thin uniform layer structure beneath Cu_6Sn_5. The Cu_3Sn intermetallic layer consistently increases with increased temperature but remains within the thickness of Cu_6Sn_5. The corrosion behavior of bare Cu, as-deposited SAC305/Cu and as-reflowed SAC305/Cu at varying reflow temperatures was investigated by means of potentiodynamic polarization in a 6 M potassium hydroxide (KOH) solution. Bare Cu was found to possess the best corrosion resistance, whereas the as-deposited SAC305/Cu had the lowest corrosion resistance. As-reflowed SAC305/Cu with an exposed Cu_3Sn layer exhibited better corrosion resistance than did Cu_6Sn_5. All of the samples contained the corrosion products of

oxide. Bare Cu obeys the well-known duplex structure of a Cu_2O/CuO, $Cu(OH)_2$ layer. For as-reflowed SAC305/Cu, the corroded surface was also mainly composed of SnO and SnO_2.

CHAPTER 1

INTRODUCTION

1.0 Introduction

Commercialization and recent advancements in integrated circuit performance have intensified packaging technology development, which resulted in an abundance of standard electronics packages. As the global trend moves towards miniaturization and high electrical performance, green manufacturing has become another challenge for electronic packaging.

Research and development of Pb-free solders is being conducted worldwide to produce environmentally friendly electronics. Transitioning to Pb-free materials has become necessary due to upcoming European legislation (Ganesan and Pecht, 2006). Intensive research on numerous Pb-free alternatives as well as their advantages and disadvantages found that Pb-free electronics assembly is technically achievable. As a result, various lead-free solders are a subject of increasing interest and growing demand.

The use of lead in soldering processes was banned in compliance with international laws. Solder plays a critical part in electronic products assembly and interconnection. As an interconnection material, solder joints perform thermal, mechanical, and electrical functions (Abtew and Selvaduray, 2000). For instance, solder serves as a die-bonding material for flip chip bonding during the solder bumping process. An intermetallic compound (IMC) layer is created at the interface as a result of the metallurgical reaction between the solder alloy and substrate

metallization. This layer is essential in maintaining solder joint integrity to prevent degradation of the assembly which is caused by the thermal stress of soldering.

Most Pb-free solders are Sn-based eutectic alloys. Because a eutectic solder alloy has a single, low melting point, the entire solder joint can melt or solidify at a temperature. Several Pb-free solders have already been proposed, including binary and ternary systems such as Sn-Cu, Sn-Au, Sn-In, Sn-Bi, Sn-Ag, and Sn-Ag-Cu which have been utilised in the electronics industry for particular applications.

Several reviews on the development of Pb-free solders were published (Abtew and Selvaduray, 2000; Glazer, 1995; Li et al., 2008; Suganuma, 2001; Vincent and Humpston, 1994), and studies on electronic assembly that uses binary Pb-free solders were summarized (Vincent and Humpston, 1994). Properties of binary Pb-free solders and technical issues of solder joints were reported (Abtew and Selvaduray, 2000), and development of ternary Pb-free solders and their interactions with metallization was conducted (Suganuma, 2001). Furthermore, substantial research and development efforts have been conducted to study the corrosion behavior of binary and ternary Pb-free solders (Glazer, 1995; Li et al., 2008). Manufacturability issues for applications of Sn-Ag-, Sn-Zn-, and Sn-Bi-based ternary solders in a low-cost electronic assembly were also presented (Glazer, 1995).

1.1 Problem Statement

Solders are used at different interconnection levels of the electronic packaging hierarchy. As a response to increasing demand for miniaturization, interconnection technology has progressed from packaged devices with conventional wire, tape

automated bonding and area-array flip chip packaging to bare die interconnection. Presently, lead-free solders are employed in solder balls, solder alloys, solder pastes, and solder wires (Islam et al., 2005b; Liu et al., 2006; Liu et al., 2009; Reid et al., 2008; Yoon and Jung, 2008). It has been extensively documented (Gong et al., 2009; Islam et al., 2005b; Kim et al., 2003; Liu et al., 2006; Liu et al., 2009; Mookam and Kanlayasiri, 2011; Yoon and Jung, 2008; Yoon et al., 2009; Yu and Wang, 2008) that Cu_3Sn and Cu_6Sn_5 IMCs formed at the interface region of bulk Sn-Ag-Cu solder and Cu substrate during soldering. For instances, interfacial Cu_3Sn and Cu_6Sn_5 IMCs are formed between some Sn-based solder alloys and a Cu under-bump metallization (UBM) (Laurila et al., 2005; Tu and Zeng, 2001) and also between organic solderability preservative (OSP) finished Cu bond-pads (Yoon and Jung, 2008). Subsequent heat treatment causes continued growth of the IMCs (Liu et al., 2009; Mookam and Kanlayasiri, 2011).

However, limited studies on thin film characteristics of Sn-Ag-Cu lead-free solders are available. Small solder volumes saturate more quickly with Cu, thus accelerating the precipitation of IMC (Frear and Vianco, 1994; Jang et al., 2004). Previous work (Bennett et al., 1980) confirmed that subsequent thermal treatments of thin solder coatings on Cu base substrates changed the surface character of the solder. The actual surface may have regions of Cu_6Sn_5 and/or Cu_3Sn which directly exposed to the environment. Consequently, the shelf life owing to solderability of components having such surfaces might be affected by the reactivity of the exposed IMCs with the environment. Hence, the reactivity of thin film characteristics need to be considered to get ready for rapidly growing trend towards electronic product miniaturization and the increasing demand for reliability.

In flip chip bonding, evaporation, screen printing, and electrodeposition are popular methods that involve depositing thin film solder alloys onto the chip bond pads (Qin et al., 2010). Diffusion soldering is another interconnection technique which involves using thin film reaction to form IMCs.

Behaviors of thin film solder alloys in corrosive environments have not yet been reported. Corrosion test data for most Pb-free solders are limited (Li et al., 2008). Electronic components are mainly exposed to different physical environments and corrosive chemical that involve ionic species such as hydroxides, potassium, sodium, and chlorides ions. Although significant efforts and preventive methods have been undertaken to protect solder joints from the effects of working environments, the joints continue to corrode due to corrosive particles and absorbed moisture that are present in the environment and which are difficult to eliminate completely. Stringent measures were implemented to decrease ionic contamination in molding compounds, and clean room chemicals were used to reduce corrosion potential (Ulrich and Brown, 2006).

Recent studies have focused on corrosion assessment of Pb-free solders in bulk alloys. Most of these studies used NaCl solution to simulate sea water (Cheng et al., 2011; Li et al., 2008; Rosalbino et al., 2009; Rosalbino et al., 2008; Wu et al., 2006). Studies have also investigated the electrochemical behavior and corrosion of tin in an alkaline media (Alvarez et al., 2002; Brunetti and López Teijelo, 2008; El Rahim et al., 1986; Gervasi et al., 1997; S.A.M, 1996). However, the performance of 96.5Sn-3.0Ag-0.5Cu (SAC305) thin film in conductive potassium hydroxide (KOH) has not been reported.

KOH is used as an electrolyte for alkaline batteries that are used in automotive and electronic devices because of its conductivity (Minami et al., 2005). Alkaline batteries are prone to leaking KOH. All batteries gradually self-discharge (whether installed in a device or not) and dead batteries will eventually leak. Extremely high temperatures can also cause batteries to rupture and leak. The reason for leaks is that as batteries discharge, either through usage or gradual self-discharge, the chemistry of the cells changes and some hydrogen gas is generated. This out-gassing increases pressure in the battery. Eventually, the excess pressure either ruptures the insulating seals at the end of the battery, or the outer metal canister, or both. In addition, as the battery ages, its steel outer canister may gradually corrode or rust, which can further contribute to containment failure.

Once a leak has formed due to corrosion of the outer steel shell, potassium hydroxide absorbs carbon dioxide from the air to form a feathery crystalline structure of potassium carbonate that grows and spreads out from the battery over time, following along metal electrodes to circuit boards where it commences oxidation of copper tracks and other components, leading to permanent circuitry damage. The leaking crystalline growths can also emerge from seams around battery covers to form a furry coating outside the device, that corrodes any objects in contact with the leaking device.

KOH is also used as alkaline detergent in ultrasonic cleaning. Thus, electrolyte leakage may also occur during ultrasonic removal of rosin flux from the surface of solder alloys by using an aqueous solution that contains alkaline detergent.

This exposes the electrical circuit to a corrosive KOH environment. Electrolyte leakage of the electrolyte could be catastrophic to the circuit.

In this work, the SAC305 thin film was deposited on Cu substrate through thermal evaporation technique which was then underwent various solder reflow conditions. A potentiodynamic polarization test was conducted for all the studied samples to examine the corrosion and electrochemical behavior of SAC305 thin film solder alloy in 6 M KOH solution. Surface morphology, elemental composition, and phase determination were conducted as well to clarify the structure-property relationship. By understanding failure mechanisms of Pb-free solders in an alkaline media, the application of lead-free solders could be more strategically designed to ensure reliability.

1.2 Objectives

The objectives of this research are:

i. To produce and study the interfacial reaction between SAC305 thin film and Cu substrate by using solder reflowing at various temperatures and times.

ii. To investigate the corrosion behavior of as-reflowed SAC305/Cu at reflow temperatures ranging from 230 – 260 ºC in KOH solution by using potentiodynamic polarization.

1.3 Scope of Work

SAC305 is the Sn-Ag-Cu solder alloy that was chosen for this study. This project is divided into two sections. The first section involves preparing the SAC305

thin film on Cu substrate and characterizing the interfacial reaction of SAC305 thin film on Cu substrate after solder reflow process at different temperatures and times. This process ensures IMC formation at the interface. In the second section, an electrochemical test was conducted on the as-reflowed SAC305/Cu at various temperatures in KOH electrolyte and the structural and microstructural properties of corroded samples were determined and discussed.

CHAPTER 2

LITERATURE REVIEW

2.0 Introduction

This chapter reviews on the role and importance of Sn-Ag-Cu in term of bulk solder alloys in electronics industry, since the studies on thin film characteristics are very limited. Therefore, the interfacial reaction of this alloy with Cu during soldering and its electrochemical properties in various corrosive solutions are reviewed.

2.1 Soldering in Electronics Technology

Soldering is a well-recognized metallurgical joining method that involves the application of filler metal, solder and heat, with a melting point below 425 ºC (Manko, 1979). Solders are heated up and completely melt during the soldering process. Here, the molten solders wet the substrates, and consequently dissolve the substrates and result in interfacial reactions between solders and substrates (Abtew and Selvaduray, 2000; Frear, 1991; Laurila et al., 2005; Wassink, 1989). The joints are then cooled down and finally solidified to form solder joints.

The soldering process can be depicted in Figure 2.1, and can be generally divided into three stages (Lea, 1988):

(a) spreading,

(b) base metal dissolution, and

(c) formation of an intermetallic compound (IMC) layer.

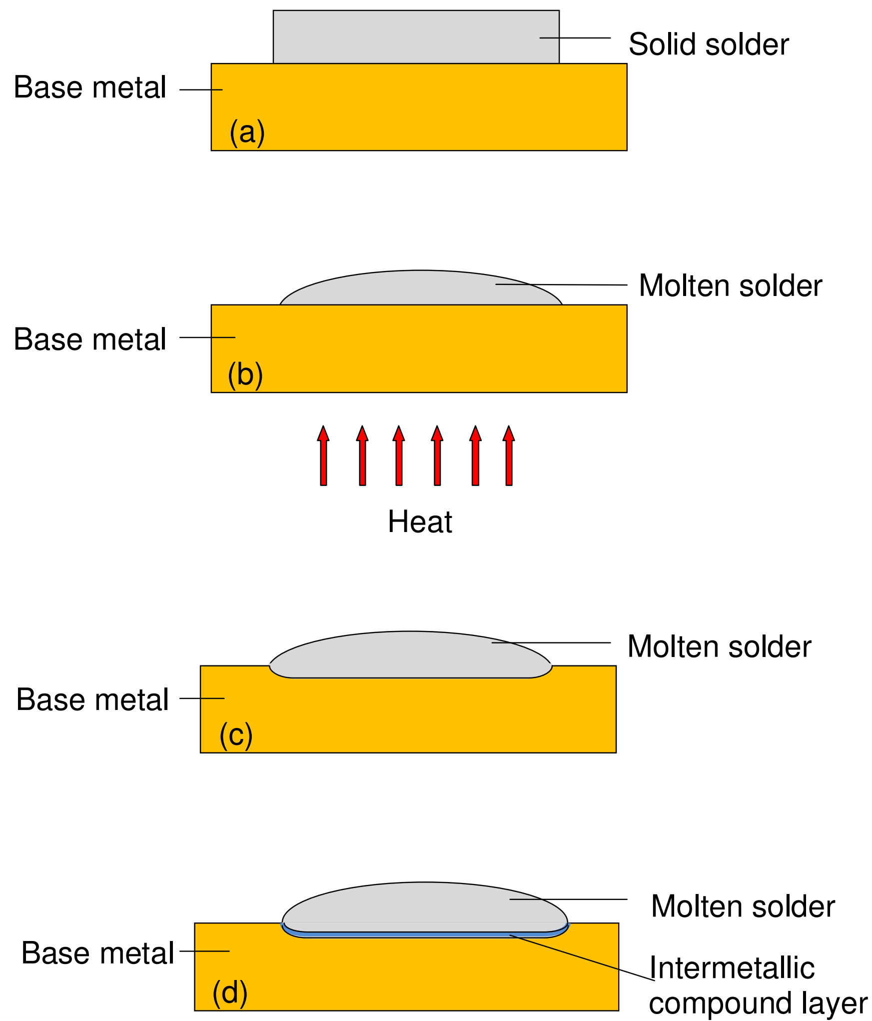

Figure 2.1: Solder wetting process: (a) solid solder on the base metal, (b) liquid solder spreading over base metal during soldering, (c) base metal dissolving in liquid solder, and (d) base metal reacting with liquid solder to form intermetallic compound layer (modified from Lea, 1988).

Moreover, soldering does not melt or change the microstructure of the base metal during joining process. During solidification, the liquid phase transforms into different solid phases which are important in determining the solder joint properties.

Since soldering is conducted at a completely molten state of solders, thus, solders are generally low melting point alloys (Chen et al., 2007a). Diffusion is significant for most solders because they are generally used at relatively high operation temperatures. In addition, good wetting is necessary, thus interfacial reactions with substrates are usually important either at the liquid/solid contacts, or at the solid/solid contacts at the operation temperatures (Chen et al., 2007a).

The solder joint strength is governed by the land pattern design and the metallurgical bond between component and board. A reliable solder connection must possess a good metallurgical bond between the solder and the components being joined. Hence, interfacial reactions at the solder joints are the crucial reliability factor of electronic products.

In the enormous electronic materials world, solder is essential in the interconnection and assembly of the silicon die. Solders are used in different interconnection levels of electronic packaging hierarchy. Many years solder plays an important role as the key means of interconnection, where the packaged device is mounted on a printed circuit board (PCB). Solder serves as joining material to provide thermal, electrical, and mechanical continuity in electronics assemblies. For example, solder is used to connect the leadframe of package to a board in circuit board manufacturing.

Virtually all microelectronic devices are mounted on PWBs using solders. There are two main methods of electronic components mounting- pin-through-hole (PTH) or surface mount technology (SMT), illustrated in Figure 2.2a and Figures

2.2b-c, respectively. Surface mounted electronic components can be divided into two designs, leaded package, as shown in Figure 2.2b or have solder balls that are known as ball grid arrays (BGAs), as presented in Figure 2.2c.

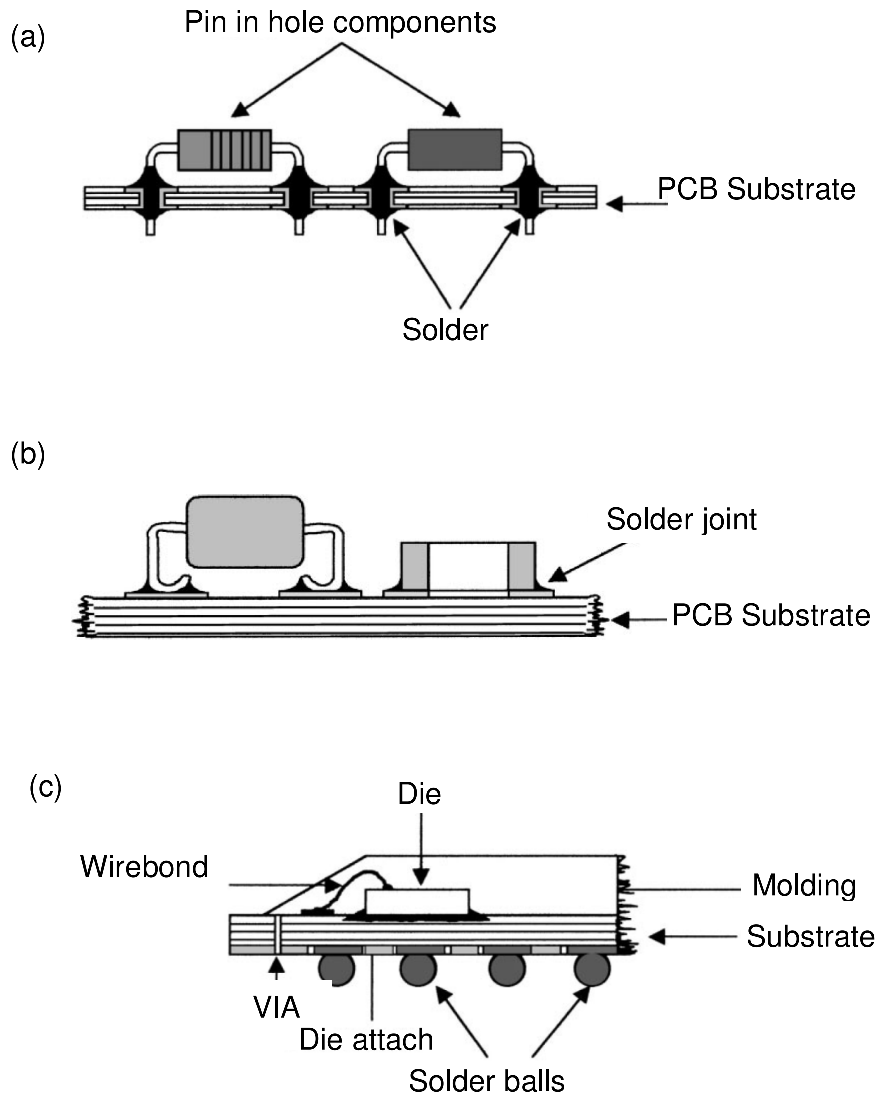

Figure 2.2: Cross-section of (a) a pin through hole connection of a microelectronics component on a printed circuit board, (b) a surface mount connection of a microelectronics component with leads on a printed circuit board, and (c) a ball grid array (BGA) microelectronics component (Abtew and Selvaduray, 2000).

As electronic packages are moving towards miniaturization, decreasing of substrate size, higher interconnect density, and more complex in geometry and material properties, the performance, quality, and reliability of the solder become essential to a solder joint integrity, which directly affect the overall functioning of the assembly and its long-term performances (Abtew and Selvaduray, 2000).

Hence, the interconnection technology route has progressed from conventional wire and tape automated bonding to area array flip chip. In the flip chip bonding technology, solder serves as a die bonding material via solder bumping process (Figure 2.3). Electrical and mechanical connection is made by solder bumps. It also serves as a heat dissipation path, generated by the semiconductor.

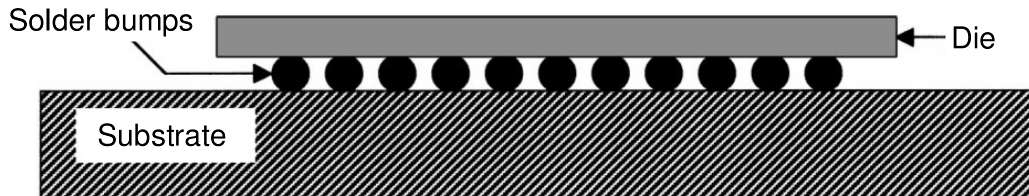

Figure 2.3: Cross-section of a flip chip connection (Abtew and Selvaduray, 2000).

Recently, different solder bumping methods have been applied in order to further achieve the increased demand on package miniaturization. The popular technologies are evaporation, screen printing and electrodeposition (Qin et al., 2010).

Evaporation is an expensive process with efficiency less than 5% while more than 95% of the evaporated material attaching on the evaporator wall and on the metal mask. Screen printing technology remains the key production method owing to its low cost and yield. Yet, screen printing is not altogether a promising method. The

demand for higher patterns density and increase of circuitry complexity has become a great challenge for future applications. Therefore, flip-chip bumping by electrodeposition is gaining interest because it achieves an overall high yield at reasonable cost (Gruber et al., 2005; Madhav, 2003).

2.2 Thin Film Solders

Following the miniaturization of electrical packaging components, the dimensions of the solders have also decreased (Hung et al., 2006). As a result, thin film technology has been introduced since thin film enables fine pitch interconnect to be fabricated. A thin film is defined as a layer of material ranging from fractions of a nanometer (monolayer) to several micrometers in thickness. Thin films play an important role in modern technology, especially in electronics as connectors, contacts and interconnections (Bukaluk, 1989).

Extensive studies of the interfacial reactions in metallic multilayers and their properties have been made. For instance, in the thin film Cu-Au system, the elements form a complete solid solution in all composition ranges, and in the Cu-Cr system the elements are almost insoluble in each other (Hansen and Anderko, 1958). Also, the deposition of Ag on Cu and Cu-based substrates has recently received considerable interest, as a result of its wide application in preparation of optical and laser mirrors. The Cu surface layer originated from diffusion through the Ag film protects the film from atmospheric contamination (Bukaluk, 1989).

However, there is little information on the Sn-Ag-Cu solder thin films. Hence, Sn-Cu thin film system (Chopra et al., 1981; Fujiwara et al., 1980) which has the

closest elemental composition to the Sn-Ag-Cu ternary alloy system is the most appropriate candidate to represent the behavior of Sn-Ag-Cu thin film. Sn-Cu thin film will be discussed and elaborated in this section. Moreover, the interdiffusion in thin films is faster than in bulk materials corresponding to a high density of defects, such as vacancies, dislocations and interfaces (Wronkowska et al., 2008). This in turn results in the rapid formation of interfacial reaction, which leads to the formation of intermetallic layer. So it is reasonable to study and review recent development and approaches in investigations of interfacial intermetallic compounds (IMCs) between Sn-Cu thin film from the metallurgical point-of-view.

The growth kinetics of Cu_6Sn_5 and Cu_3Sn compounds in Cu/Sn thin film couples by in situ resistivity measurement during isochronal annealing from room temperature to 220 °C was studied (Liao and Wei, 2006). The authors found that Cu_6Sn_5 grows and dominates at lower temperature, ranging from room temperature to 206 ºC). No Cu_3Sn phase was found at low temperature due to very small critical thickness. However, Cu_3Sn compound starts to grow and increase in thickness at the expense of the Cu_6Sn_5 phase with rising temperature to 220 ºC.

Solid-liquid interdiffusion bonding (SLID) is another interconnection technique based on the principle of isothermal solidification. During the process, the low-melting metallic thin-film interlayer which melts at low temperatures will reacts rapidly with both high-melting layers or with substrates to form IMCs. The interfacial IMCs possess much higher melting points than the original low-melting interlayer, thus allow bonding at lower temperatures and usage at higher temperatures (Bader et al., 1995).

A fluxless Cu/Sn SLID bonding process was demonstrated by using intermetallic Cu_3Sn layer as the oxidation barrier for Cu interconnects (Liu et al., 2010a). The approach for the flip chip bonding in this experiment is shown in Figure 2.4, where the interconnect pads of Cu/Sn are bonded to pads of Cu/Cu_3Sn. All the Cu and Sn thin films in this work were deposited by electroplating procedures using Cu-sulphate and Sn sulphate-based electrolytes, respectively, which allows the fabrication of fine-pitch interconnects at relatively low cost. These have make Cu-Sn based SLID bonding a very promising interconnection technique for 3D stacked applications (Huebner et al., 2006).

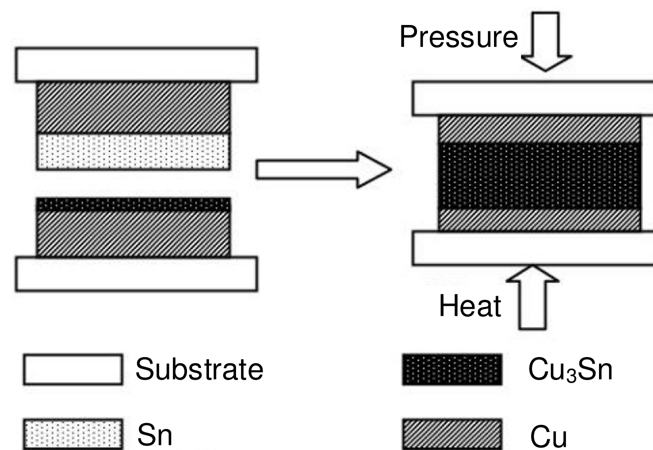

Figure 2.4: Illustration of fluxless bonding with a thin Cu_3Sn layer as the oxidation barrier (Liu et al., 2010a).

Liang et al. (2003) studied the applicability of thin film reactions during diffusion soldering of Cu/Ti/Si and $Au/Cu/Al_2O_3$ with Sn interlayers, as schematically shown in Figure 2.5. Experimental results showed that a double layer of IMCs η-$(Cu_{0.99}Au_{0.01})_6Sn_5$/$\delta$-$(Au_{0.87}Cu_{0.13})Sn$ was formed at the interface. Kinetics

analyses revealed that the intermetallics growth was diffusion-controlled and eventually, attaining a satisfactory tensile strength of 132 $kgcm^{-2}$.

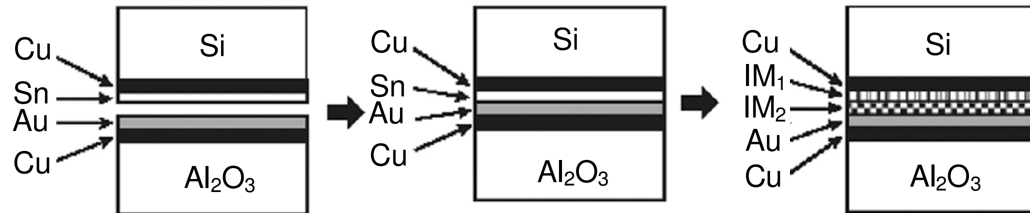

Figure 2.5: The scheme of diffusion soldering for Cu/Ti/Si and Au/Cu/Al_2O_3 with Sn interlayers (Liang et al., 2003).

2.3 Sn-Ag-Cu Solders

Sn-Ag-Cu alloys have been recognized as the most promising lead-free solder candidate among the various alloy systems being considered, because of their superior mechanical properties, good compatibility with common commercial components, and relatively low melting temperature (compared with the Sn-Ag binary eutectic lead free solder) (Kim et al., 2003; Yoon et al., 2005; Yu and Wang, 2008). Sn-Ag-Cu alloys are widely used as lead-free solutions for ball-grid-array (BGA) interconnection in the microelectronic packaging industry as solder ball and solder paste (Farooq et al., 2001).

With regard to the bumping materials, a family of solder alloys based on the ternary Sn-Ag-Cu eutectic (217 ºC) composition has emerged with the most potential for broad use across the industry (Kang et al., 2006). Eutectic composition is favourable to be chosen as it behaves as an independent homogenous phase and has a unique metallographic structure and distinct melting point (Manko, 2001b). Sn-Ag-Cu solders enhance joint strength and creep and thermal fatigue resistance, and

enable to sustain at increased operating temperatures for advanced electronic systems and devices (Subramanian, 2007; Wu et al., 2004). The International Printed Circuit (IPC) Association has suggested that the 96.5Sn–3.0Ag–0.5Cu (SAC305) and Sn–3.9Ag–0.6Cu (two near-eutectic alloys) will be the most widely used world-wide (Wu et al., 2004). This is attributed to the good mechanical properties, acceptable wetting properties and suitable melting points of this alloy (Li et al., 2005; Wang and Chen, 2006; Yoon et al., 2005; Yu and Wang, 2008).

In fact, it was reported that the formation of small-dispersed particles in lead-free solder joints revealed fine and stable microstructures which in turn, result in higher shear strengths (Li-Lei et al., 2000). Sn-Ag-Cu solders require higher reflow temperature. The melting point of Sn-3.8Ag-0.7Cu is 219 ℃, and that of SAC305 is 217 ℃. The high melting temperature requires a new reflow profile, and also increases the component stability concerns accompanying with the higher temperature. Some components may not survive at that high reflow temperature.

2.3.1 Phase diagram of Sn-Ag-Cu solders

The phase diagram of Sn-Ag-Cu system (Figure 2.6a) was experimentally determined and no ternary phases have been reported (Gebhardt and Petzow, 1959). Meanwhile, the solid phases have fairly small ternary homogeneity ranges. Recent work (Loomans and Fine, 2000; Miller et al., 1994) showed that this is eutectic reaction with a temperature of 217 ± 0.2 °C, and the liquid decomposes into Sn and the binary intermediate compounds Ag_3Sn and Cu_6Sn_5. The calculated tin-rich part of the liquidus projection is shown in Figure 2.6b. The interception of red-dashed lines corresponds to 96.5Sn-3.0Ag-0.5Cu (SAC305).

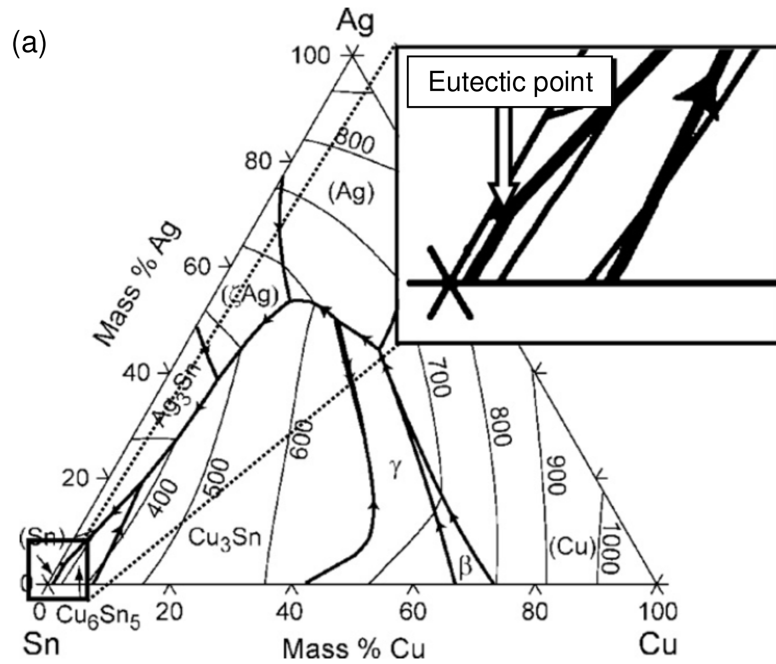

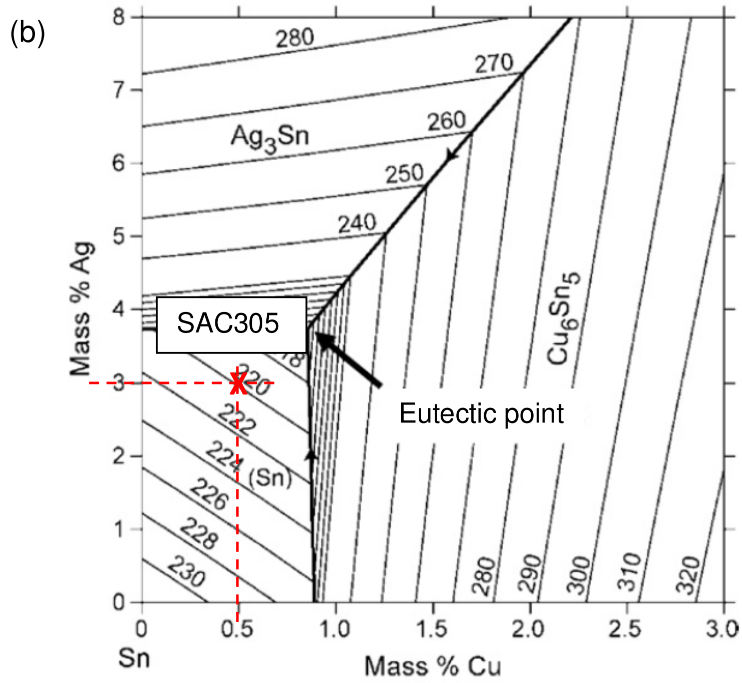

Figure 2.6: (a) Ternary phase diagram of Sn-Ag-Cu solder alloy and (b) liquidus surfaces of Sn-Ag-Cu phase diagrams at the Sn-rich corner (Moon et al., 2000).

As shown in Figure 2.7 of the Sn–Ag binary system, the composition of Ag_3Sn comprises of Sn varying between 25.5 and 26 wt%. The solid solubility of Ag in Sn is less that 0.1 wt%.

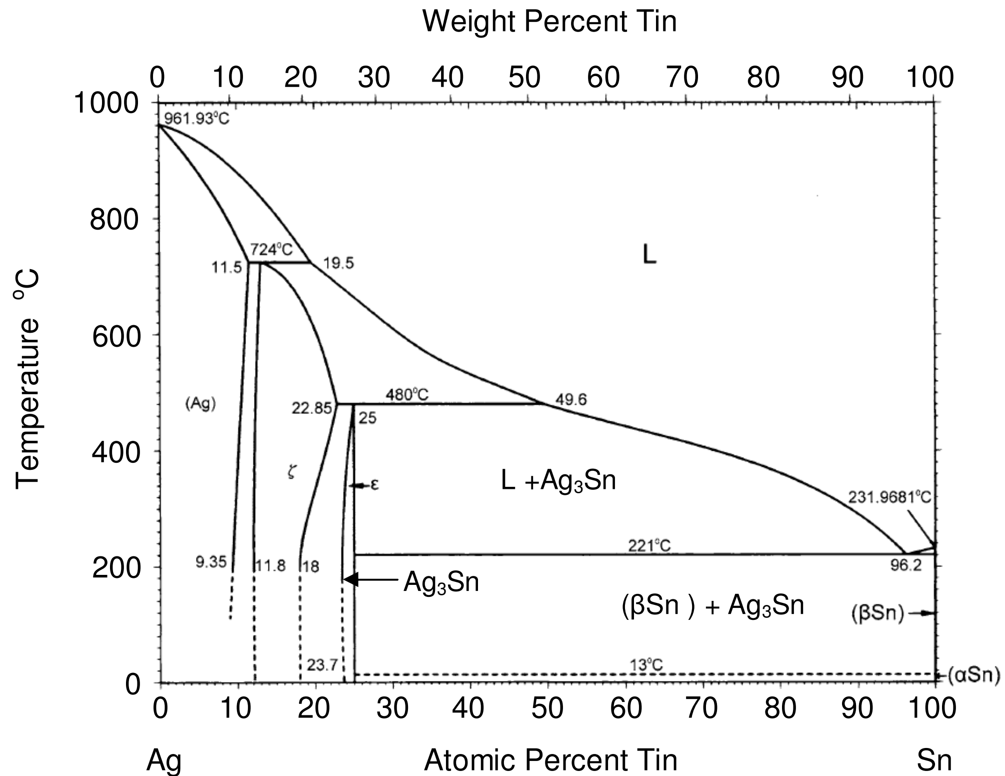

Figure 2.7: Binary Ag-Sn system (Massalski and Okamoto, 1990).

From the phase diagram of Cu-Sn (Figure 2.8), the ε-Cu_3Sn and η-Cu_6Sn_5 intermetallic phases are stable below 300 ºC. The ε-Cu_3Sn phase has a composition range between 25.7 and 27.1 wt% Sn. Meanwhile, the η-Cu_6Sn_5 phase has Sn concentration ranging between 44.8 and 45.5 wt%. The growth of these phases follows the Arrhenius relationship, with the activation energy for Cu_6Sn_5 being between 0.41 and 0.5 eV while for Cu_3Sn being between 1.06 and 1.27 eV, in the 90-

170 ℃ range (Dunn et al., 1985), suggesting that the growth of Cu_6Sn_5 would be faster than Cu_3Sn under these temperature conditions.

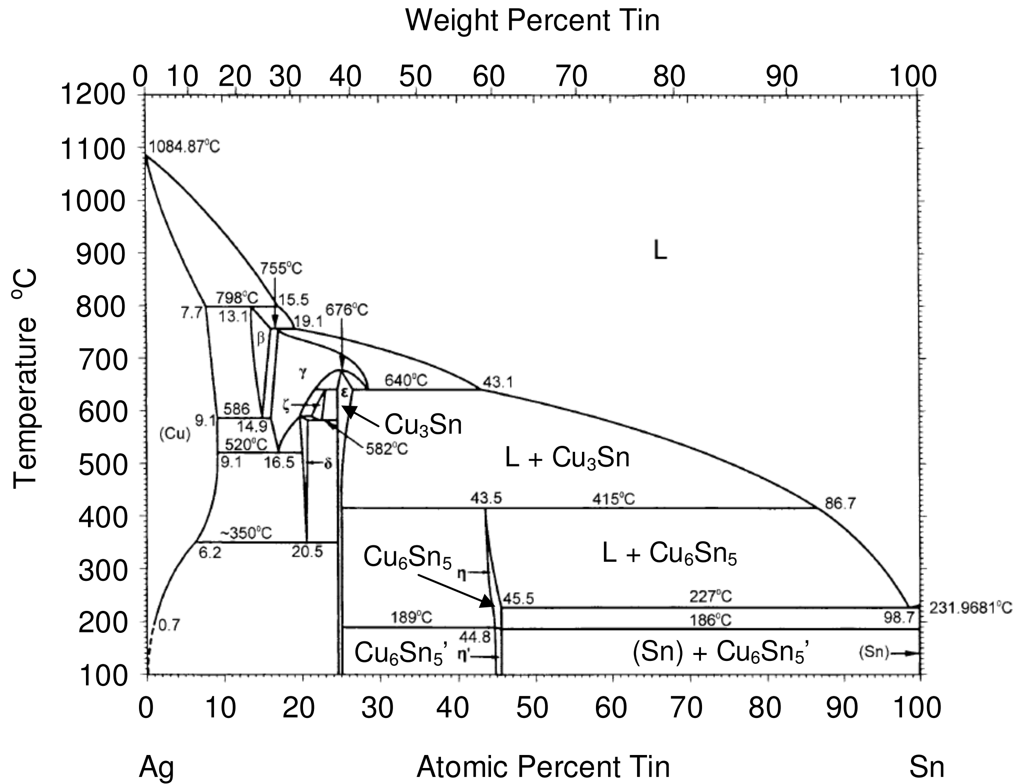

Figure 2.8: Cu-Sn binary phase diagram (Massalski and Okamoto, 1990).

2.4 Intermetallic Compound of Sn-Ag-Cu Solders with Cu Substrate

All the common base materials, metallizations, and coatings used in electronic products such as Ag, Cu, Au, Ni, and Ag–Pd, formed IMCs with Sn. Therefore, during soldering, chemical reactions occur between solders and conductor metals (i.e. boards surface finishes, underlying conductors, and component metallizations) and IMCs will nucleate and grow at the solder/conductor interfaces.

The presence of the IMCs between solders and conductor metals indicates good metallurgical bonding. The reliability of solder joints is mainly dependent on the interfacial IMC layer (Jang et al., 2004). So attention has to be paid to the effect of IMCs growth on the lifetime and reliability of microelectronic assemblies. A thin, continuous and uniform IMC layer is a vital requirement for good bonding. On the other hand, in absence of IMCs, the solder/conductor joint is weak because no metallurgical interaction in the bonding, which is disastrous to electronic packaging.

However, during storage and field service, the growth of IMCs will influence the strength of solder joints and result in mechanical failure of the joints [6 –10]. Our recent research result shows that the fatigue lifetime of solder joint decreases linearly with the increasing square root of IMCs layer thickness [11]. A thick IMC layer at the solder/conductor metal interface may degrade the solder joints reliability, correspond to their inherent brittle behavior and the tendency to generate structural defects resulted by mismatches of the physical properties (such as elastic modulus and coefficient of thermal expansion) (Nai et al., 2009).

Under certain conditions, it is essential to determine what thickness of solders is sufficient. Manko (2001a) reported that the formation of IMC with thickness of 1–2 μm between the solder and UBM is considered an indicator of good metallurgical bond and wetting. Thus, the metallurgical viewpoints and knowledge of the solder/conductor metal interactions and phase evolution in the solder interconnections, are important for the understanding of the reliability of the solder interconnections and for the optimization of the soldering process (Laurila et al., 2005).

The intermetallic reaction layers are formed in three consecutive stages (Laurila et al., 2005):

(a) dissolution,

(b) chemical reaction, and

(c) solidification.

During the soldering of Sn-Ag-Cu solder on the Cu substrate, instantaneously after the flux has removed the oxides and permits metallurgical contact between the solder and contacted Cu, the Cu starts to dissolve rapidly to the molten solder. Initially the dissolution rate is very high. The dissolution is non-equilibrium and very high concentration of Cu locally in Cu/liquid interface. After a short duration of time, the layer of molten solder which is adjacent to the contacted Cu becomes supersaturated with the dissolved Cu throughout the interface.

Thermodynamically, at the local equilibrium solubility, the solid IMC starts to form in the layer of the solder that is adjacent to the contacted metal. Since there's a large driving force for chemical reaction between Cu and Sn atoms at the metastable composition, Cu_6Sn_5 crystallites formed. Scallop-type Cu_6Sn_5 first formed at Sn/Cu interface during soldering and its occurrence is very fast. Cu_6Sn_5 is formed by dissolution of Cu followed by chemical reaction. If contact with molten solder is long enough, Cu_3Sn formed between Cu_6Sn_5 and Cu. Cu_3Sn is formed by diffusion and reaction type growth (Kivilahti, 2002).

Figure 2.9 briefly illustrates the interfacial reaction of SAC305/Cu during solder reflow. When heat is applied, the solid SAC305 solder melts and the contacted Cu substrate starts to dissolve to the molten SAC305 solder (Figure 2.9a). The layer

of molten SAC305 solder near to the SAC305/Cu interface becomes supersaturated with the dissolved Cu (Figure 2.9b). The solid IMC begins to form at the interfacial zone. Cu_6Sn_5 with scallop structure forms firstly (Figure 2.9c) followed by formation of thin layer-like Cu_3Sn (Figure 2.9d).

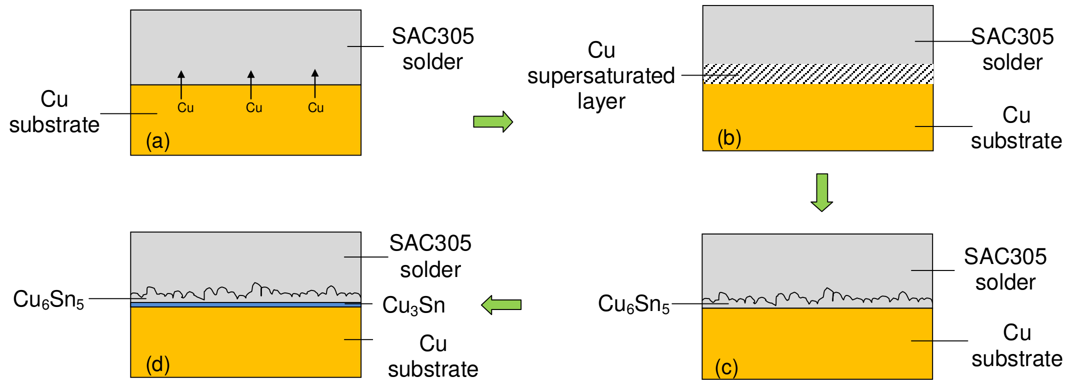

Figure 2.9: Scheme of the interfacial reaction of SAC305/Cu during solder reflow; (a) dissolution of Cu substrate, (b) supersaturation of molten solder layer with Cu, (c) formation of scallop type Cu_6Sn_5 at interface, and (d) Cu_3Sn emerges between Cu_6Sn_5/Cu with prolonged soldering (modified from Kivilahti, 2002).

2.4.1 Structural phases of Sn-Ag-Cu/Cu

Cu is the most frequent conductor used in connection with solders, owing to its excellent thermal conductivity performance and superior solderability characteristic (Rizvi et al., 2006). Liu et al. (2010b) investigated the interfacial reactions between SAC305 solder paste and Cu substrate at 250 ºC and 300 ºC from 30 s up to 1800 s. Ag_3Sn particles were detected on SAC305/Cu interface after soldering (Figure 2.10). The authors explained that Ag atoms react with Sn to form Ag_3Sn phase in liquid solder at the initial stage. Then, precipitation of Ag_3Sn phase

occurred near the IMCs which are prone to be "captured" by the IMCs during solidification process. In addition, the IMC structure in liquid state remains unchanged in the solid state if only small increase of the liquid temperature than the melting temperature.

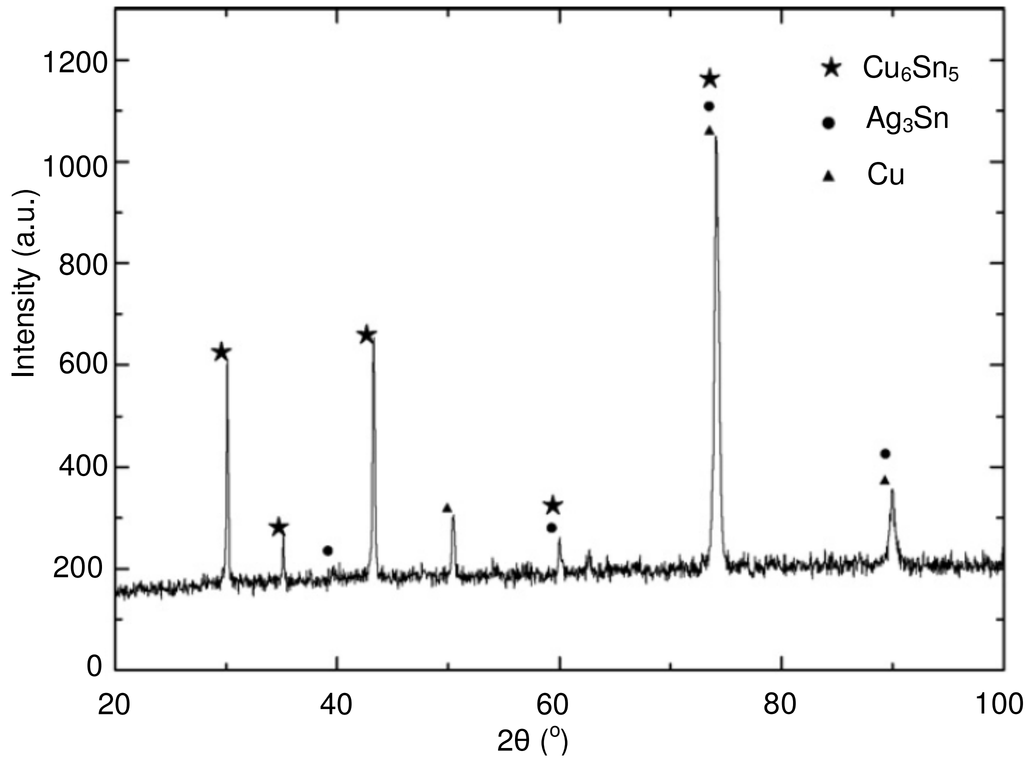

Figure 2.10: XRD patterns of interfacial IMC at SAC305/Cu joints reflowed at 250 ºC for 30 s (Liu et al., 2010b).

Besides that, the XRD analysis of interfacial SAC305/Cu was performed by Wang et al. (2007) to examine the phase structure of IMC during soldering at 260 ºC for 20 s, as shown in Figure 2.11. The XRD pattern indicates that the crystal structure of IMCs for SAC305/Cu is Cu_6Sn_5.